NUMERICAL MODELING OF DROPLET TRAJECTORIES AND COLLECTION EFFICIENCY USING THE LAGRANGIAN APPROACH

TÍNH TOÁN SỐ QUỸ ĐẠO CỦA HẠT NƯỚC VÀ HỆ SỐ BÁM SỬ DỤNG TIẾP CẬN LAGRANGE

Duong De Tai*

Tran Dai Nghia University, Vietnam

*Corresponding author: duongdetai@gmail.com

(Received: August 22, 2025; Revised: October 15, 2025; Accepted: Novemver 17, 2025)

DOI: 10.31130/ud-jst.2025.23(11).398E

Abstract - The paper presents a numerical method for investigating the motion of supercooled water droplets in airflow using the Lagrangian approach. The method is employed to compute droplet trajectories and capture efficiency on solid surfaces under two-phase flow conditions. Simulations are carried out on canonical geometries, including a cylinder (2D) and a sphere (3D), representing typical aircraft components such as sensors or leading edges. The computed results are compared with available experimental data and show strong agreement within acceptable confidence intervals. Furthermore, a novel approach is proposed to transform discrete droplet impact data into a continuous field representation of capture efficiency. This enables improved visualization and analysis of droplet impingement, serving as an essential step toward accurate simulation of icing processes on aircraft surfaces. Besides, a droplet seeding method with appropriate spacing in the Lagrangian framework is proposed to ensure sufficient accuracy in the calculation of the capture coefficient.

Key words - Lagrangian approach; supercooled water droplet; droplet motion equations; capture coefficient; ice accretion

Tóm tắt - Bài báo trình bày phương pháp số khảo sát chuyển động của các giọt nước siêu lạnh trong dòng không khí sử dụng tiếp cận Lagrange. Phương pháp được áp dụng để tính toán quỹ đạo và hệ số bám của giọt nước lên bề mặt vật thể trong điều kiện dòng chảy hai pha. Mô phỏng được thực hiện trên hình học cơ bản gồm hình trụ (2D) và hình cầu (3D), đại diện cho các thành phần của thiết bị bay như cảm biến, hoặc mép trước cánh. Kết quả được so sánh với thực nghiệm cho thấy sự tương đồng cao. Ngoài ra, bài báo đề xuất một phương pháp mới để chuyển dữ liệu va chạm rời rạc của các giọt thành trường liên tục mô tả hệ số bám, giúp nâng cao khả năng trực quan và phân tích hiện tượng bám giọt – một bước quan trọng trong mô phỏng quá trình đóng băng trên bề mặt. Bên cạnh đó, một phương pháp gieo hạt với khoảng cách hợp lý trong không gian cũng được đề xuất nhằm đảm bảo đủ độ chính xác khi tính toán hệ số bám bề mặt.

Từ khóa - Tiếp cận Lagrange; hạt siêu lạnh; phương trình hạt nước; hệ số bám; đóng băng

1. Introduction

Icing on aircraft remains one of the significant safety hazards for civil aviation today. Icing occurs when aircraft fly through clouds containing supercooled particles in sub-zero temperatures [1]. The ice accumulation on aerodynamic surfaces reduces lift and increases drag [2] but can also change the shape of the wing and create adverse vibration phenomena, leading to aerodynamic instability [3]. In addition, ice also distorts signals from sensors such as pitot tubes or angle-of-attack vanes, leading to the risk of losing flight control [4-6]. Therefore, accurately predicting the location and density of water droplet impacts on the surface is key to optimizing sensor placement and designing effective anti-icing systems.

Over the past three decades, many models have been developed to simulate the motion and adhesion of water droplets to aircraft surfaces. The two primary widely used methods are Eulerian and Lagrangian [7]. The Eulerian approach considers the droplet phase a continuum and solves conservation equations for liquid water content and its velocity on a fixed grid [8-9]. This method is suitable for large-scale problems. However, it often lacks accuracy in predicting the trajectories of individual droplets, especially in the case of large droplet sizes or low concentrations, or when the cloud contains many particles of different sizes [10].

In contrast, the Lagrangian method tracks individual droplets by solving the equations of motion according to Newton's second law under the influence of aerodynamic drag, gravity, and other inertial effects [11]. This approach accurately determines impact locations and capture coefficient on aircraft surfaces and is the basis of many ice simulation tools such as LEWICE, TRAJICE2D [12-14]. However, most of these tools still focus on two-dimensional models which reduces accuracy when applied to complex three-dimensional geometries [15].

Recent studies have extended the Lagrangian method to more realistic conditions, including 3D geometries (e.g., spheres, realistic wing models), supercooled large droplets (SLDs) [16-17]. However, a problem exists that collision data from Lagrangian simulations are inherently discrete, making it difficult to compare them with continuous data from experiments quantitatively. The lack of a method to convert particle impinging data to a continuous scalar field is a significant gap in this field. In addition, in the Lagrange method, the trajectory of each particle is tracked from when the particle is at the free-stream until the particle hits the surface or moves behind the object. However, how to choose the position of the particles at infinity to be suitable and optimal for calculating the trajectory and adhesion coefficient has not been discussed.

This study aims to address these gaps by presenting a fully Lagrangian framework for simulating droplet impingement on both 2D (cylinder) and 3D (sphere) bodies. We validate our results against benmark experimental data, demonstrating that the computed capture efficiencies fit within experimental confidence bounds. More importantly, we propose a novel technique for converting discrete droplet impact data into a continuous capture efficiency field, improving interpretability, and facilitating comparison with experimental data, and propose a seeding strategy for supercooled droplets at the inlet to ensure accurate calculation of the capture coefficient. So, the key contributions of this work are as follows:

- Implementation of a high-order Lagrangian droplet tracking method for 2D and 3D geometries;

- Quantitative comparison of computed capture efficiency with experimental data;

- Seeding strategy for supercooled droplets at the inlet;

- Development of a method to convert particle impact data into continuous field representation.

By focusing exclusively on the Lagrangian approach, this study provides a clear, efficient, and extensible framework for analyzing droplet impingement in complex geometries. The results have significance for safer sensor placement, enhanced ice protection strategies, and future integration with thermodynamic icing models.

2. Equation of motion of supercooled droplets

The governing equations for the air - water two-phase flow (air with supercooled water droplets) are derived under the following assumptions: (i) there is no energy exchange between the droplets and the air; (ii) the droplets are small (≤ 40 μm), remain spherical, and do not deform while moving through the air. With no energy coupling, the air acts on the droplets only through aerodynamic drag and buoyancy (Archimedes force). Therefore, the air–droplet problem can be solved in a decoupled manner. First, the airflow is computed to obtain the flow field (velocity, pressure, temperature, viscosity, etc.) on the grid. Next, this flow field is used to compute the droplet motion. The forces on each droplet include three components: drag, gravity, and buoyancy. The aerodynamic drag force $\vec{F}_D$ on a supercooled droplet is given by [18]:

$$\vec{F}_D = \frac{1}{2}\rho_a \vec{u}_r^2 A C_D = \frac{\pi}{8}\rho_a d^2 |\vec{u}_a - \vec{u}_d|(\vec{u}_a - \vec{u}_d) C_D \quad (1)$$

where $A = \pi(d/2)^2$- is the droplet cross-sectional area; $d -$ is the droplet diameter (often referred to as MVD - mean volume diameter); $\rho_a, \vec{u}_a -$ are the air density and air velocity; and $C_D -$ is the aerodynamic drag coefficient.

The local Reynolds number of droplets is:

$$Re_d = \frac{\rho_a d}{\mu}|\vec{u}_a - \vec{u}_d| \quad (2)$$

Solving $\rho_a|\vec{u}_a - \vec{u}_d|$ from the Eq. (2) and substituting into the Eq. (1):

$$\vec{F}_D = \frac{\pi}{8}\mu d(\vec{u}_a - \vec{u}_d) C_D Re_d \quad (3)$$

where μ is the air viscosity at the location of the considered water droplet.

The gravitational force $\vec{F}_g$ and the Archimedes buoyancy $\vec{F}_B$ are:

$$\vec{F}_g = m_d \vec{g} = \Omega_d \rho_w \vec{g};\ \vec{F}_B = -\Omega_d \rho_a \vec{g} \quad (4)$$

where $\vec{g} = (0, -g, 0) -$ is the gravity vector; $\rho_w = 1000\ kg/m^3 -$ is the density of water and $\Omega_d = \frac{4}{3}\pi R^3 = \frac{4}{3}\pi\left(\frac{d}{2}\right)^3$ is the volume of the supercooled droplet.

Applying Newton's second law (sum of forces equals rate of change of momentum) gives the supercooled droplet equation of motion:

$$m_d \vec{a} = \sum \vec{F} \rightarrow m_d \frac{d\vec{u}_d}{dt} = \vec{F}_D + \vec{F}_g + \vec{F}_B \quad (5)$$

Inserting Eqs. (2) - (4) into Eq. (5) yields:

$$\frac{d\vec{u}_d}{dt} = \frac{0.75\mu C_D Re_d}{\rho_w d^2}(\vec{u}_a - \vec{u}_d) + g\left(1 - \frac{\rho_a}{\rho_w}\right) \quad (6)$$

Equation (6) is the equation of motion for a water droplet in an airflow. It is general and applies to particles of any size. For small droplets, the particle is assumed spherical, the well-known drag coefficient formula $C_D Re_d$ developed by Langmuir and Blodgett [18] is used:

$$\frac{C_D Re_d}{24} = 1 + 0.197 Re_d^{0.63} + 2.6 \times 10^{-4} Re_d^{1.38} \quad (7)$$

Note that Eq. (7) is valid only for $Re_d \leq 1000$.

3. Numerical method

The governing equation for the motion of a droplet in an airflow (Eq. 7) can be expressed in the general form:

$$\frac{d\vec{u}_d}{dt} = f(t, \vec{u}_d), \vec{u}_d|_{t=0} = \vec{u}_0$$

where u_d represents the state variable (e.g., velocity vector of the droplet), t is time, and $f(t, \vec{u}_d)$ encapsulates the physical forces acting on the particle, including aerodynamic drag, gravity, and buoyancy.

For time integration, to improve accuracy, we implemented a second-order scheme based on the predictor–corrector [19]:

- Predictor step:

$$\hat{u}_d = u_d^n + \tau f(t_n, u_d^n)$$

- Corrector step:

$$u_d^{n+1} = u_d^n + \frac{\tau}{2}[f(t_n, u_d^n) + f(t_n + \tau, \hat{u}_d)]$$

The corresponding local truncation error (LTE) is:

$$\psi_n = -\frac{u_d^{n+1} - u_d^n}{\tau} = -\frac{\tau^2}{2}u_n'' + O(\tau^3)$$

demonstrating second-order temporal accuracy, where halving the time step reduces the error by a factor of approximately four.

The droplet position was updated via:

$$x_d^{n+1} = x_d^n + \tau u_d^n$$

This scheme provides a balanced compromise between numerical accuracy and computational efficiency, making it particularly suitable for tracking droplet trajectories in complex flow fields.

4. Study of water droplet flow around a cylinder

In both experimental analysis and numerical simulations, the collection efficiency β serves as a key parameter for quantifying the ability of a surface to capture incoming water droplets. For Eulerian-based approach, the formulation of β is defined as the ratio of the local water mass flux to the freestream water mass flux [12], as described in Eq. (8):

$$\beta = \frac{\rho_n v_n}{\rho_\infty v_\infty} \quad \text{q} \tag{8}$$

where ρ_n is the local droplet density on the surface, v_n is the component of droplet velocity normal to the surface, and ρ_∞, v_∞ are the corresponding freestream values.

In the Lagrangian approach, droplet trajectories are tracked individually. Since the droplet field is inherently discrete, a definition of continuous liquid water content (LWC) is not possible. Instead, β is determined from the deformation of droplet trajectory spacing between the freestream and the surface [13]:

$$\beta = \frac{dy}{ds} \tag{9}$$

where, dy is the distance between two closely spaced trajectories at infinity, and ds is the distance along the surface of the solid between the two corresponding trajectories (Figure 1).

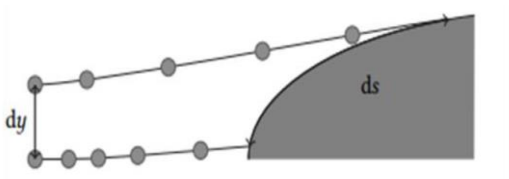

Figure 1. *Capture coefficient in 2D*

Note that when $\beta = 1$, the spacing between two trajectories remains the same at the inlet and on the body surface. This mean that the liquid water content of droplets between the two trajectory is conserved. At a certain position, the capture coefficient becomes zero. This location is called the "tail". Above the tail, droplets do not impinge on the surface at all. The determination of the capture coefficient (Eq. 9) is a crucial step in the Lagrangian approach, as it serves as a fundamental parameter in solving the thermodynamic icing problem.

In this section, a set of the trajectories of water droplets in the flow around a cylinder was investigated. The air flow field is described using the potential flow solution [20]:

$$v_r^a = v_\infty \left(1 - \frac{R_0^2}{r^2}\right) \cos\theta \; ; \; v_\theta^a = -v_\infty \left(1 + \frac{R_0^2}{r^2}\right) sin\,\theta$$

Initial parameters for air and water droplets are: cylinder radius $R_{cyl} = 0.0508\,m$; droplet mean volume diameter $MVD = 16\,\mu m$; free-stream velocity $v_a = 80\,m/s$; liquid water content (droplet desity) $\rho_d = 0.55\,g/m^3$; gravity $g = 9.81\,m/s^2$; ambient temperature pressure are $t_\infty = 12℃$; $p_\infty = 89867\,Pa$. These parameters were taken from the experiment in [21].

The results of the calculations of droplets are shown in Figure 2. Point A marks the "tail", above which droplets do not hit the cylinder. The limit angle was found as 40.9195°. Point B is defined as the "stagnation point". The droplet trajectories impinging on the surface are recorded, and capture coefficients are calculated.

The obtained capture coefficient distribution on the cylinder is compared with experimental data [21] and with numerical results using the Euler (FVM) approach. The comparison is shown in Figure 3. Experimental results are plotted with black lines. The Lagrangian results are shown with red circles, and the Euler results with blue triangles. In the plots, the x-axis is the cylinder surface coordinate (Oy), and the y-axis is the capture coefficient β.

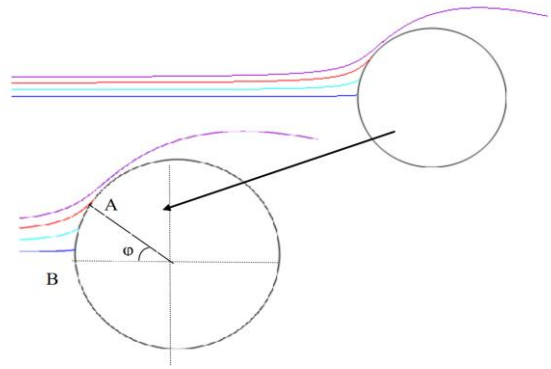

Figure 2. *Trajectories of water droplets in the air flow field around a cylinder*

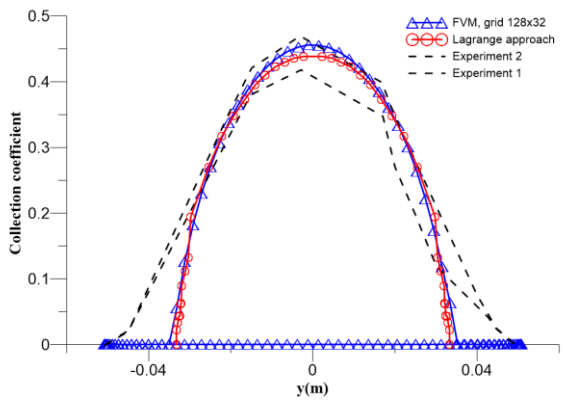

Figure 3. *Collection coefficient on cylinder*

The β values at the stagnation point and at the leading edge of the cylinder, calculated using the Lagrangian method, are within the error range of the experimental data. A noticeable difference appears only in the tail region, where the results deviate from the experiments. This issue will be discussed in Section 6 after the analysis of the 3D cylinder. The β distributions obtained from the Lagrangian and Euler methods are almost the same. The two-dimensional Lagrangian approach offers both simplicity and computational efficiency. It enables rapid determination of droplet trajectories and allows straightforward implementation in numerical algorithms. More importantly, the method has been validated against experimental data, demonstrating its reliability for practical applications.

5. Study of water droplet flow around a sphere

The three-dimensional case is considered to be the flow of water droplets around a sphere with the following

parameters: $R_{sphera} = 0.0752\ m$; $MVD = 18.6\ \mu m$; $v_a = 75\ m/s$; $\rho_d = 0.55\ g/m^3$; $t_\infty = 7°C$; $p_\infty = 95840\ Pa$. These parameters were taken from the experiment in [22].

To obtain the droplet trajectories, the airflow field is first required. This field is obtained from inviscid flow around a sphere using the Ansys CFX program. Figures 4 and 5 present the velocity and pressure distributions of the airflow around the sphere. Based on the air flow field, the droplet trajectories are then computed. In Section 4, the formula for the capture coefficient in two-dimensional space (Eq. 9) was presented. In three-dimensional space, the formula is slightly different. The capture coefficient in the Lagrangian approach is expressed as Eqs (10):

$$\beta = \frac{S_\infty}{S} \tag{10}$$

where S_∞, S are the areas of four closely located droplets at infinity and on the surface of a solid [m^2], respectively (see Figure 6). Formular in Eq. (10) shows the ratio between the initial area of the droplets far from the body and the final area of the droplets that actually reach the surface.

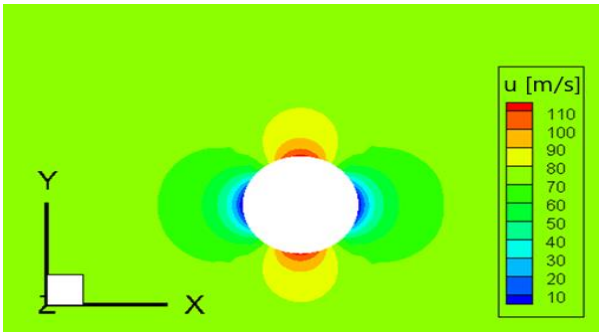

Figure 4. *Distribution of the velocity component field along the Ox axis around the sphere in section $z = 0$*

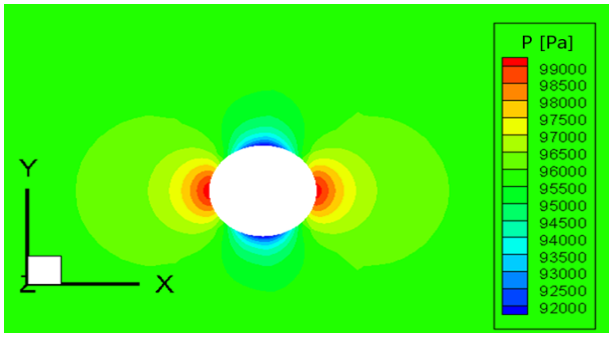

Figure 5. *Distribution of the pressure field around a sphere in cross-section $z = 0$*

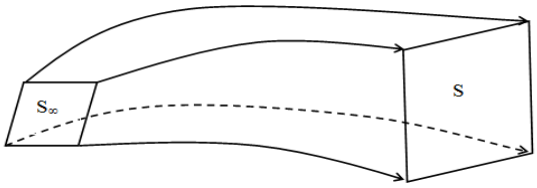

Figure 6. *Picture of four droplet trajectories at infinity and on the surface of a body*

To calculate the capture coefficient β, four closely spaced droplet trajectories are required. The choice of these points is important. If the initial area is too small, the calculation becomes long and inefficient. If the area is too large, the β may be estimated incorrectly. In this study, the points are selected based on physical considerations. Assume that the water field has a liquid water content ρ_d, the mass of each droplet is given by Eqs (11):

$$m_d = \rho_w V = \rho_w \frac{4}{3}\pi R_d^3 \tag{11}$$

where $\rho_d = 0.55\ gr/m^3$; and the droplet radius is $R_d = 9.3\ \mu m$. In a unit volume of $1\ m^3$, the number of droplets is N^3, where N is the number of droplet in each direction Ox, Oy, Oz (see Figure 6).

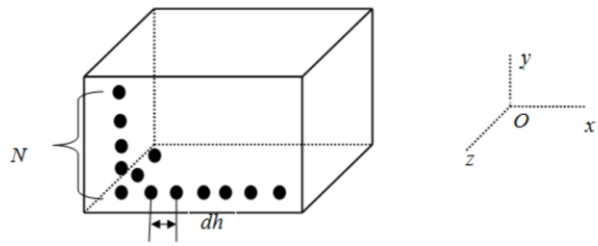

Figure 6. *Distribution pattern of water droplets per unit volume*

The distance between the two neighboring droplets is $dh = \frac{1}{N}$ with $N^3 = \frac{\rho_d}{m_d} \rightarrow dh = R^3\sqrt{\frac{4\pi}{3}\frac{\rho_w}{\rho_d}} \approx 1.83 \times 10^{-3} m$. Once the four initial droplet positions are set, the trajectories are calculated. The capture coefficient on the sphere surface is then obtained. In Figure 7, the blue lines represent the trajectories of droplets that do not strike the sphere surface, while the black lines correspond to the droplets that impact the surface. Near the sphere surface, the trajectories are compressed and move closer together, indicating an increase in droplet density in this region. This local increase in droplet density directly contributes to the capture coefficient and explains t

he higher liquid water content on the sphere surface. From these positions, the capture coefficient is estimated from Eq. (10).

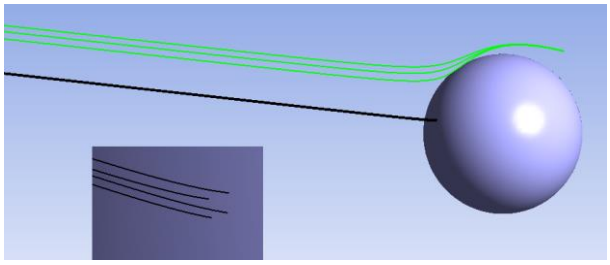

Figure 7. *Droplet trajectories in space*

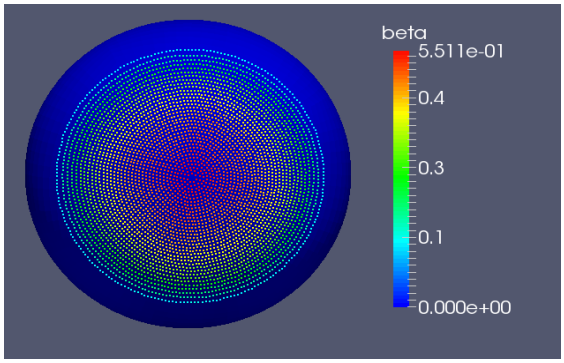

Figure 8. *Capture coefficient on the surface of a sphere*

Figure 8 shows the capture coefficients on the surface of a sphere. The colored dots are the centers of the areas formed by four closely spaced droplets hitting the sphere. These central points are called “particles”.

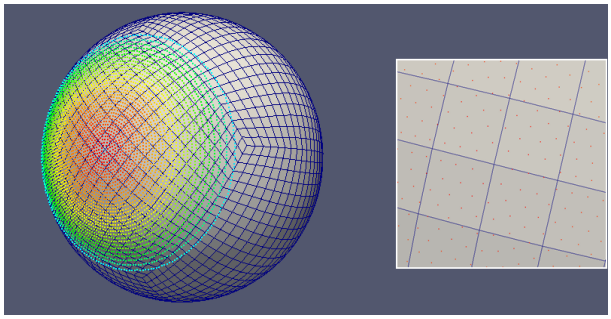

Figure 9. *The arrangement of "particles" in a grid cell*

In Figure 9 some “particles” in grid cell is shown. The average value of the capture coefficient in one grid cell is calculated by Eqs (12):

$$\bar{\beta} = \frac{\sum_{j=1}^{N_i} \beta_{ij}}{N_i} \tag{12}$$

where β_{ij} is the capture coefficient of the $j-th$ particle in the $i-th$ cell, and N_i is the number of particles in that cell. The value of the capture coefficient at the grid node is estimated by Eqs (13):

$$\beta_{node} = \frac{\sum_{i=1}^{K_{node}} \beta_i \Omega_i}{\sum_{i=1}^{K_{node}} \Omega_i} \tag{13}$$

where K_{node} is the number of cells surrounding the node, Ω_i is the volume of the $i-th$ cell.

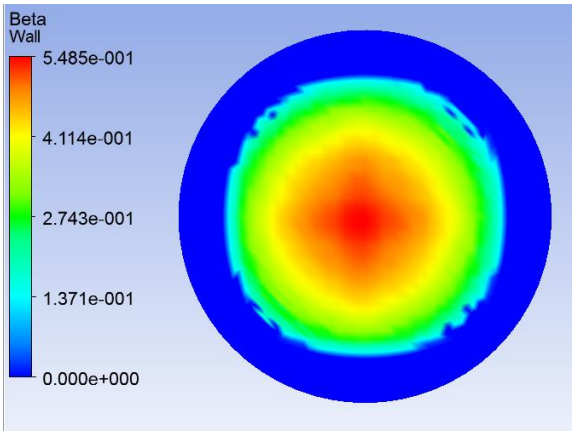

Figure 10. *The capture coefficient β at the nodes of the sphere surface*

Figure 10 shows the distribution of capture coefficients at the grid nodes. The results are compared with experiments and with the Euler approach. Figure 11 shows this comparison for the section $z = 0$. The black lines are experimental data [22]. The red line with triangles is the Euler result. The blue line with circles is the Lagrangian result. The coefficient at the stagnation point agrees well with the experiment, but the value in the tail region shows a larger deviation. This difference is related to the flow behavior. In real flow, unsteady vortices (Karman vortices) are formed, and the separation points change over time. In the simulation, however, the air flow is steady and inviscid (Figures 4 and 5), and no vortex shedding is present. Because the droplet trajectories are computed from this steady airfield, the difference in the capture coefficient between experiment and simulation becomes clear, especially in the tail region. This highlights the limitation of the steady inviscid model in capturing unsteady separation effects, which are important for accurate icing predictions.

The results in Figure 11 also show that the Lagrangian method gives values very close to the Euler approach in the stagnation region. The relative difference is about:

$$\sigma = \frac{\beta_{stag}^{Lag} - \beta_{stag}^{Eul}}{\beta_{stag}^{Eul}} = 4.046\%$$

where β_{stag}^{Lag}, β_{stag}^{Eul} are the capture coefficients at the stagnation point from the Lagrangian and Euler methods, respectively. This small difference confirms the reliability of the method.

From the obtained results we conclude that the Lagrangian method performs reliably in three-dimensional space. It can therefore be applied to evaluate the water field parameters, including liquid water content ρ_d, and velocity components (V_x, V_y, V_z) in all cells and nodes of the grid.

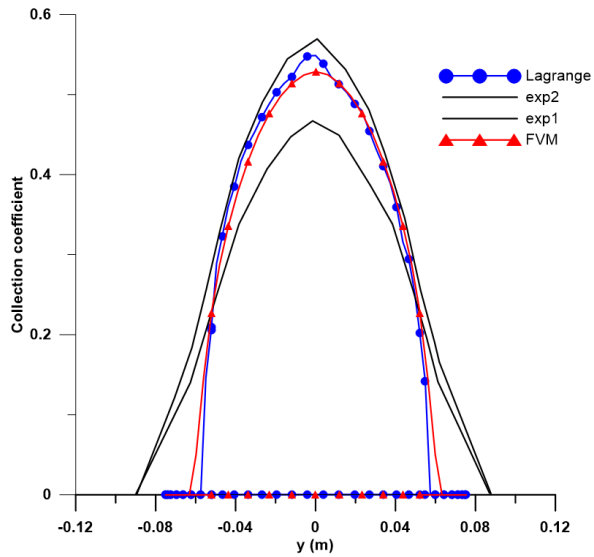

Figure 11. *The capture coefficient β in the section z=0*

6. Conclusion

This study developed a Lagrangian method for simulating the motion of supercooled droplets and their capture efficiency on solid surfaces. The method was validated against experiments in both two-dimensional (cylinder) and three-dimensional (sphere) cases and show good agreement with experimental data, especially in the stagnation region, while some deviations occur in the tail region due to the steady inviscid flow assumption.

A new interpolation technique was proposed to convert discrete droplet impact data into a continuous capture efficiency field. This improves visualization and makes comparison with experimental results easier. In addition, a droplet seeding strategy with appropriate spacing was introduced to ensure accuracy in the calculation of the capture coefficient.

Overall, the Lagrangian approach provides a reliable and efficient tool for predicting droplet trajectories and capture efficiency in icing studies. It can be applied to calculate key water field parameters, including liquid water content and velocity components, across both two- and three-dimensional geometries. These results highlight the potential of the method for improving the accuracy of aircraft icing simulations.

REFERENCES

[1] R. W. Gent, N. P. Dart, and N. P. Dart, "Aircraft icing", *Phil. Trans. R. Soc. A*, vol. 358, 2000. https://doi.org/10.1098/rsta.2000.0689

[2] Y. Cao, C. Ma, Q. Zhang, and J. Sherida, "Numerical simulation of ice accretions on an aircraft wing", *Aerospace Sci. and Tech.*, vol. 23, issue 1, pp. 296-304, 2012. https://doi.org/10.1016/j.ast.2011.08.004

[3] F. T. Lynch and A. Khodadoust, "Effects of ice accretions on aircraft aerodynamics", *Progress in Aerospace Sciences*, vol. 37, issue 8, pp. 669–767, 2001. https://doi.org/10.1016/S0376-0421(01)00018-5

[4] L. Xianglian *et al.,* "Pitot Tube-Based Icing Detection: Effect of Ice Blocking on Pressure", *Int. J. of Aerospace Eng.*, vol. 2020, no. 1, 2020. https://doi.org/10.1155/2020/1902053

[5] Q. Chen and C. Zhou, "Numerical Simulation Study on Predicting the Critical Icing Conditions of Aircraft Pitot Tubes", *Sensors*, vol. 24, issue. 22, 2024. https://doi.org/10.3390/s24227410

[6] C. Raab and N. Fezans, "Measuring the angle of attack - practical considerations for the development of fault detection residuals", in *34-th Congress of the International Council of the Aeronautical Sciences (ICAS)*, Florence, Italy, 2024. https://www.icas.org/icas_archive/icas2024/data/papers/icas2024_0156_paper.pdf

[7] R. Meireles, L. Magalhaes, A. Silva, and J. Barata, "Description of a Eulerian-Lagrangian Approach for the Modeling of cooling water droplets", *Aerospace*, vol. 8, issue 9, 2021. https://doi.org/10.3390/aerospace8090270

[8] H. Beaugendre, F. Morency, and W. G. Habashi, "FENSAP-ICE's Three-Dimensional In-Flight Ice Accretion Module: ICE3D", *J. of Aircraft*, vol. 40, issue 2, 2003. https://doi.org/10.2514/2.3113

[9] Y. Bourgault, W. G. Habashi, J. Dompierre, Z. Boutanios, and W. Di Bartolomeo, "An Eulerian approach to supercooled droplets impingement calculations", in *35th Aerospace Sciences Meeting and Exhibit (AIAA Paper 97-0176),* Reno, USA, 1997. https://doi.org/10.2514/6.1997-176

[10] A. Shad, H. Ahmed, N. Zgheib, S. Balachandar, and S. A. Sherif, "Stokes-dependent droplet collection efficiency on a NACA0012 airfoil from droplet-informed simulations with statistical overloading", *Phil. Tran. R. Soc. A*, vol 383, 2025. https://doi.org/10.1098/rsta.2024.0368

[11] L. Xie, P. Li, H. Chen, and H. Liu, "Robust and efficient prediction of the collection efficiency in icing accretion simulation for 3D complex geometries using the Lagrangian approach I: an adaptive interpolation method based on the restricted radial basis functions", *Int. J. Heat and Mass Transfer*, vol. 150, 2020. https://doi.org/10.1016/j.ijheatmasstransfer.2019.119290

[12] C. S. Bidwell and M. G. Potapczuk, "*Users manual for the NASA Lewis Three-Dimensional Ice Accretion Code (LEWICE 3D)*", research project report, NASA, USA, NASA-TM-105974, 1993. https://ntrs.nasa.gov/citations/19940017117.

[13] R. W. Gent, "*TRAJICE 2 - A combined water droplet trajectory and ice accretion prediction program for aerofoils*", research project report, RAE, England, RAE TR 90054, 1990.

[14] W. B. Wright, "*DRA/NASA/ONERA Collaboration on Icing Research. Part II-Prediction of Airfoil Ice Accretion*,", research project report, NASA, USA, NASA CR 202349, 1997. https://ntrs.nasa.gov/citations/19970023937

[15] H. Beaugendre, F. Morency, and W.G. Habashi, "FENSAP-ICE's Three-Dimensional In-Flight Ice Accretion Module: ICE3D", *J. of Aircraft*, vol. 40, no. 2, 2003. https://doi.org/10.2514/2.3113

[16] S. Ozgen and E. B. Saribel, "Modeling of Supercooled Large Droplet Physics in Aircraft Icing", *Aerospace*, vol. 11, no. 10, 2024. https://doi.org/10.3390/aerospace11100797

[17] H. Han, Z. Yin, Y. Ning, and H. Liu, "Development of a 3D Eulerian/Lagrangian Aircraft Icing Simulation Solver Based on OpenFOAM", *Entropy*, vol. 24, no. 10, 2022. https://doi.org/10.3390/e24101365

[18] J. M. Hospers, "*Eulerian method for super-cooled large-droplet ice-accretion on aircraft wings*", Ph.D. dissertation, Faculty of Engineering Technology, University of Twente, Netherlands, 2013. https://doi.org/10.3990/1.9789036536172

[19] J. D. Freed, "*A Technical Note: Two-Step PECE Methods for Approximating Solutions To First- and Second-Order ODEs*", research project report, Cornell University, USA, 2017. https://doi.org/10.48550/arXiv.1707.02125

[20] J.D. Anderson, *Fundamentals of Aerodynamics*, 6th edition. NJ: McGraw-Hill Education, 2017.

[21] X. Tong and E. Luke, "Eulerian Simulations of Icing Collection Efficiency Using a Singularity Diffusion Model", in *43rd AIAA Aerospace Sciences Meeting and Exhibit (AIAA 2005-1246)*, Reno, USA, 2005. https://doi.org/10.2514/6.2005-1246

[22] Y. Bourgault, Z. Boutanious, and W. G. Habashi, "Three-dimensional Eulerian Approach to Droplet Impingement Simulation Using FENSAP – ICE, Part 1: Model, Algorithm, and Validation", *J. of Aircraft*, vol. 37, no. 1, 2000. https://doi.org/10.2514/2.2566.